Supplementary Information

Abnormal size effect enables ampere-level O_2 electroreduction to hydrogen peroxide in neutral electrolyte

Shan Ding,[a] Baokai Xia,[a] Ming Li,[a] Fengqian Lou,[a] Chi Cheng,[b] Tianqi Gao,[a] Yuxiang Zhang,[a] Kang Yang,[a] Lili Jiang,[a] Zhihao Nie,[a] Hongxin Guan,[a] Jingjing Duan,[a] and Sheng Chen*[a,b]

[a]Key Laboratory for Soft Chemistry and Functional Materials (Ministry of Education), School of Chemistry and Chemical Engineering, School of Energy and Power Engineering, Nanjing University of Science and Technology, Ministry of Education, Nanjing, 210094, China

[b] Department of Chemical Engineering, University of Melbourne, Parkville, Victoria, Australia

Correspondence and requests for materials should be addressed to:

sheng.chen@njust.edu.cn (S.C.)

I. Experimental Section

1.1 Chemicals

Zinc acetate dihydrate (Zn $(CH_3COO)_2$ $2H_2O$, AR, 99%), sodium hydroxide (NaOH, AR, 99%), cethyltetraethylammonium bromide (CTAB, AR, 99%), gelatin, potassium sulfate (K_2SO_4, AR, 98%), were purchased from Aladdin Reagent and directly used without further treatment or purification. Nafion solution (5 wt%) were brought from Alfa Aesar. Gas diffusion electrode (GDE, Shanghai Hesen). All aqueous solutions were prepared with high-purity de-ionized water (DI-water, resistance 18.25 MΩ cm^{-1}).

1.2 Synthesis of S-, M- and L-ZnO crystals

In a typical chemical bath deposition (CBD) procedure, 60 mL of 0.2 M zinc acetate dihydrate (Zn $(CH_3COO)_2$ $2H_2O$) aqueous solution and 60 mL of gelatin (0 ~ 175 μM) were prepared, respectively. Next, the above solutions were mixed and reacted at 95 °C for 6 hrs. The as-produced products were washed with copious DI-water, centrifuged and freeze dried.

1.3 Physical characterizations

Scanning electron microscopy (SEM) was performed on a field emission scanning electron microscope (FESEM, JEOL 7800F); Energy-dispersive X-ray spectroscopy (EDS) and element mapping were conducted on SEM (OXFORD X-Max^N 150 10 KV); Transmission electron microscope (TEM) was conducted on an aberration-corrected TEM (FEI Titan 80-300, 300 KV acceleration voltage). X-ray diffractions were performed on X-ray diffractometer with Cu- Kα radiation (XRD, Smartlab 9 KW, 40 KV, 40 mA, Cu Kα radiation, λ=1.5418 Å); X-ray photoelectron spectroscopy (XPS) was collected between 0 and 1350 eV on an Axia Ultra (Thermo ESCALAB 250XI) XPS spectrometer equipped with an Al Kα source (1486.6 eV);

Atomic force microscope (AFM) was performed on Bruker D8 SPM. *In-situ* Raman was conducted on a HORIBA LabRAM HR Evolution Raman spectrometer with a 532 nm solid laser as an excitation source. Inductively coupled plasma mass spectrometry element analysis (ICP-MS) was conducted on an Agilent 7800 (RF Power:1300 W; Pump rate: 29 r min^{-1}; Nebulizer flow: 0.86 L min^{-1}; Auxiliary gas: 0.7 L min^{-1}; Sample flush time: 40 s).

1.4 The ORR activities evaluated on rotating ring-disk electrode (RRDE) system.

The measurement has been operated on a RRDE configuration (Pine Research Instrumentation, USA) consisting of a glassy carbon disk electrode and a platinum ring electrode. The working electrodes were prepared by solution-casting method. Firstly, 5 mg of catalyst, 0.5 mg of acetylene black, 30 μL of Nafion (5 wt%) were dispersed in 1 mL of isoproponal/ DI-water (3:1 v/v) by sonication for 1 hr to form a uniform catalyst ink. Next, 10 μL of the ink was dropped onto a rotating ring-disk electrode (electrode area: 0.2475 cm^2) to form a uniform catalyst layer, which were then dried under ambient condition overnight. A standard three-electrode system was assembled by using the rotating ring-disk electrode loaded with catalyst as the working electrode, a Pt counter electrode and a saturated Ag/AgCl (saturated KCl) reference electrode. The ORR activities and selectivity were studied by linear sweep voltammetry (LSV) at the rotation speed of 1600 rpm with the fixed potential of +1.2 V (*vs*. RHE) in the Pt ring to detect the as-generated H_2O_2 from the disk electrode in O_2-saturated 0.6 M K_2SO_4. electrolyte.

The H_2O_2 molar selectivity (%) was determined by comparing the disk current and H_2O_2 oxidation current at the Pt ring according to the following equation:

$$\text{Molar selectivity of } H_2O_2 \text{ (\%)} = \frac{n_{H2O2}}{n_{H2O2}+n_{H2O}} = \frac{200\times\frac{\text{Ir}}{\text{N}}}{|\text{Id}|+\frac{\text{Ir}}{\text{N}}}$$

The H$_2$O$_2$ Faradaic efficiency (FE) of H$_2$O$_2$ was calculated from the disk current (I_d) and ring current (I_r) of the RRDE according to the following equation:

$$\text{Faradaic efficiency of H}_2\text{O}_2\ (\%) = \frac{100 \times \frac{Ir}{N}}{|Id|}$$

and the number of electrons transferred (n) can be obtained by the following equation:

$$\text{The number of electrons transferred n} = \frac{4 \times |Id|}{|Id| + \frac{Ir}{N}}$$

Where I_d is disk current, I_r is ring current, and N is the current collection efficiency of RRDE, which was determined to be 0.37.

All the measured potentials were converted to reversible hydrogen electrodes (RHE) according to $E_{RHE} = E_{Ag/AgCl} + 0.059$ pH$+0.197$.

1.5 The ORR activities evaluated on flow-type electrolytic cells

A flow-type electrolytic cell system was applied to evaluate the potential for practical H$_2$O$_2$ production. The working electrode was prepared by solution casting method. In detail, 5 mg of catalysts, 0.5 mg of acetylene black, 30 μL of Nafion solution (5 wt%) were dispersed in 1 mL of isoproponal/ DI-water (3:1 v/v) by ultrasonication for 1 hr to form a uniform catalyst ink. Next, 1 mL of the homogeneous catalyst ink was sprayed on a 1×1 cm^2 gas diffusion electrolyte (GDE). The electrocatalytic test were conducted on a CHI 760E electrochemical workstation connected with a CHI 680C high current amplifier. This standard three-electrode three-phase flow cell was assembled by employing ZnO GDE (1×1 cm^2) as working electrode, titanium-based metal oxide coated electrode (DSA, 2×2 cm^2, IrO$_2$ coating) as counter electrode, and Ag/AgCl (saturated KCl) as reference electrode. Nafion 117 membrane was used as a proton exchange membrane (PEM) to separate the cathode

and anode compartments. 0.6 M K_2SO_4 aqueous solution was used as the catholyte and anolyte, which was circulated through the flow cell by using a peristaltic pump at a rotate speed of 40 rpm, and O_2 was fed into the gas chamber with a continuous flow rate of 80 mL min^{-1}.

All the electrochemical data was presented without *iR* correction, the current densities were normalized to the geometrical area. The calculation for hydrogen peroxide yield rate (mg h^{-1} cm^{-2}) and Faradaic efficiency (FE) were described as follows:

$$Y (H_2O_2) = c(H_2O_2) \times V / (t \times S)$$

$$FE_{H2O2} (\%) = 2F \times c(H_2O_2) \times V / (34 \times Q)$$

Where $c(H_2O_2)$ is hydrogen peroxide concentration, V is the volume of electrolyte, t is reaction time, S is the electrode area, F is the Faradaic constant, Q is the amount of electricity passed.

Further, the H_2O_2 concentration was measured by a traditional titration method based on the mechanism that a colorless solution of $Ti(SO_4)_2$ would be oxidized by H_2O_2 to H_2TiO_4 with yellow colour.

$$Ti^{4+} + H_2O_2 + 2H_2O \quad H_2TiO_4 + 4H^+$$

Thus, the concentration of H_2O_2 after the reaction can be measured by UV-Vis spectroscopy. The principle is that the concentration of the solution is proportional to the ultraviolet absorbance at 408 nm.

2. Density functional theory computational details

Computations were conducted by using density functional theory (DFT) with spin polarization. The first-principles calculations were performed by the MedeA-Vienna Ab initio Simulation Package (VASP) in view of DFT methods[1,2]. The Perdew-Burke-Ernzerhof (PBE) generalized gradient approach (GGA)[3,4] was utilized to define the

exchange-correlation potential. The interaction between the atomic cores and electrons was described by using the projector augmented wave (PAW)[5,6] pseudopotentials. The cut-off energy for plane wave expansion was set to be 400 eV, optimized from a range of a range cut-off energies. The Monkhrst-Pack K-point mesh of the Brillouin Zone in real space was sampled with $1 \times 1 \times 1$ for all calculations. The convergence criterion was set to be 0.05 eV/Å and 10^{-5} eV for force and energy, respectively, within the RMM-DIIS method for geometry optimization. The vacuum layer is set to be 15 Å to avoid interaction between two neighboring periodic cells. Hubbard-U correction approach (DFT+U) was carried out to improve the description of highly correlated Zn 3d orbitals with the value of U-J set to be 2.5 eV.

The detailed Gibbs free energy calculation for ORR has been carried out as follows:

$$G = E - TS + ZPE + G_U$$

where G, E and ZPE refer to chemical potential (partial molar Gibbs free energy), electronic energy and zero-point energy, respectively. $G_U = -eU$, in which e is the charge transferred in each elementary step and U is the applied electrode potential. The entropy term can be expressed as the sum of the translational, rotational, vibrational and electronic contributions as to:

$$S = S_t + S_r + S_v + S_e$$

Since $S_e \approx 0$ at the fundamental electronic level.

For the case of solids and adsorbates, some approximations can be adopted:

1. As for gases, at the fundamental electronic level $S_e \approx 0$[7].

2. Translational and rotational motions can be omitted, therefore, $S_t \approx 0$ and $S_r \approx 0$. In this case, all the entropy values come from the vibrational contribution: $S = S_v$. Similarly, translational and rotational contributions to heat capacity are neglected.
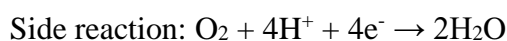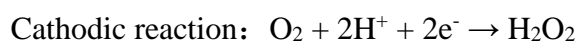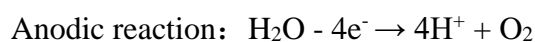
Ultimately, Gibbs free energy for different states were calculated as to:

$$G = E - TS_v + ZPE + G_U$$

3. Techno-economic assessments

3.1 Process simulation

In this part, most process simulations were realized by software (for example, DWSIM, COCO and MATLAB). But the chemical reaction of electrolysis process is complex, and cannot find build-in models. Therefore, we have designed custom model according to two-electron-transfer ORR to H_2O_2 (please see Fig. S17, ESI). The possible reactions inside the electrolysis device are listed follows:

Anodic reaction：$H_2O - 4e^- \rightarrow 4H^+ + O_2$

Cathodic reaction：$O_2 + 2H^+ + 2e^- \rightarrow H_2O_2$

Side reaction: $O_2 + 4H^+ + 4e^- \rightarrow 2H_2O$

According to the experiment results, seldom H_2 has been generated in the whole reaction process, so the side reaction is determined as four-electron-transfer ORR (for example, the FE of O_2-to-H_2O_2 through two-electron-transfer ORR is 98.48%, and consequently the FE of O_2-to-H_2O through four-electron-transfer ORR is 1.52%). The change of reaction heat has also taken into account due to the enthalpy difference between products and reactants in the electrolysis device.

According to the practical production demand, the process flowsheet has been built (please see Fig. S18, ESI). The reaction area of H_2O_2 electrolysis is 500 m^2. The electrolyte is aqueous K_2SO_4 solution. Non-random two liquid (NRTL) model is applied to the electrolyte system. The input of streams is shown in Table S7. Considering the running state of flow stock, the circulation of electrolyte is set as 25000 kg/hr. Further, since the utilization rates of gases are usually smaller than 20%, the circulation amount of gas is set as 15000 kg/hr.

In addition, the reaction current is calculated as:

$$I = I_S \times s_{rea}$$

Where I is the total current, I_s is the current density and s_{rea} is the reaction area.

The production of H_2O_2 is calculated according to Faraday law by taking account of the key substances are O_2, H_2O_2 and H_2O:

$$m = \frac{I \times M \times t \times FE}{n \times F}$$

Where m represents the mass of H_2O_2 (g), M is the molecular mass of H_2O_2, Q is the electricity quantity (C), I is current (A), t is time (s), and n is the electron transfer number of the reaction.

3.2 Economic analysis

3.2.1 Verify the accuracy of the simulation models.

The accuracy from simulation models has been firstly evaluated by comparing with our own calculations according to Faraday law. For L-ZnO, it can promote electrochemical reduction from O_2 to H_2O_2 with FE of 98.48% at the current density is 1 A cm^{-2}. If we aim to produce H_2O_2 with a concentration of 70 wt%,

The total current is:

$$I = I_S \times s_{rea} = 1\frac{A}{cm^2} \times 500 \text{ m}^2 \times \frac{10000 \text{ cm}^2}{m^2} = 5000000 \text{ A}$$

The power needed is given as:

$$power = UI = 3.9726 \text{ V} \times 5000000 \text{ A} = 19863000 \text{ W} = 19863 \text{ kW}$$

The yield rate of H_2O_2:

$$m/hr = \frac{I \times M \times t \times FE}{n \times F \times 1 \text{ hr}} = \frac{5000000 \text{ A} \times 34 \text{ g/mol} \times 3600 \text{ s} \times 98.48\%}{2 \times 96485 \text{ C/mol} \times 70\% \times 1 \text{ hr}}$$
$$= 4461815.678 \text{ g/hr} = 4461.82 \text{ kg/hr}$$

It is assumed the byproduct is H_2O ($O_2 + 4H^+ + 4e^- \rightarrow 2H_2O$), so the flow rate is:

$$\text{byproduct}(H_2O) = \frac{I \times M \times t \times FE}{n \times F \times 1\ hr}$$

$$= \frac{5000000\ A \times 18\ g/mol \times 3600\ s \times 1.52\%}{4 \times 96485\ C/mol \times 1\ hr} \times 2 = 25521.065\ g/hr$$

$$= 25.521\ kg/hr$$

The cathode needs to separate 4461.82 kg/hr 70 wt% H_2O_2, that is, the amount of H_2O required is:

$$\text{The cathode theory requires } H_2O = 4461.82\ kg/hr \times (1 - 70\%)$$

$$= 1338.546\ kg/hr$$

Because the byproduct is H_2O:

$$\text{The actual need to replenish } H_2O = 1338.546\ kg/hr - 25.521 kg/hr$$

$$= 1313.025\ kg/hr$$

Because both the main and the side reactions consume O_2, the theoretical value of O_2 required in 1 hour is:

$$\text{The consumption of oxygen} = \frac{m_{H_2O_2} \times M_{O_2}}{M_{H_2O_2}} \times 1 + \frac{m_{H_2O} \times M_{O_2}}{M_{H_2O}} \times \frac{1}{2}$$

$$= \frac{4461.82\ kg/hr \times 0.7 \times 32\ g/mol}{34\ g/mol} \times 1$$

$$+ \frac{25.521\ kg/hr \times 32\ g/mol}{18\ g/mol} \times \frac{1}{2} = 2962.238\ kg/hr$$

The H_2O consumption for the anodic OER reaction is:

$$\text{Anode}(H_2O) = \frac{I \times M \times t \times 2}{n \times F} = \frac{5000000\ A \times 18\ g/mol \times 3600\ s \times 2}{4 \times 96485\ g/mol \times 1\ hr}$$

$$= 1679017.464\ g/hr = 1679.017\ kg/hr$$

The O_2 for the anodic OER reaction is:

$$\text{Anode}(O_2) = \frac{I \times M \times t}{n \times F \times 1\ hr} = \frac{5000000\ A \times 32\ g/mol \times 3600\ s}{4 \times 96485\ g/mol \times 1\ hr}$$

$$= 1492459.968\ g/hr = 1492.460\ kg/hr$$

The above calculations consist well with our simulation results (please see Fig. 4 and Table S9), thus confirming the accuracy of the simulation models.

3.3 Calculation of capital input cost

From the DOE H_2A analysis for central grid electrolysis, the electrolysis cost for the stack component is $1619 m^{-2}. So we set the instillation factor as 1.2. Consequently, the cost for the reference electrolysis is:

$$\text{Electrolyzer cost} = 500 \text{ m}^2 \times \frac{\$1619}{\text{m}^2} \times 1.2 = \$971400$$

From the H_2A, the balance of plant capital cost is 35% of the total cost, while the stack is 65%:

$$\text{Bop capital cost} = \$971400 \times \frac{0.35}{0.65} = \$523061.539$$

The capital cost of membrane separation is estimated based on distillation.

$$\text{Membrane separation cost} = \$10664000 \times (\frac{428.509 \text{ L/min}}{1000 \text{ L/min}})^{0.7} \times 0.7$$
$$= \$4124578.851$$

We depreciate the cost of fixed capital to each year with a period of 20 years of project operation, and the interest rate is 3.25%.

$$\text{Depreciation of fixed capital}$$
$$= \frac{(\$971400 + \$523061.539 + \$4124578.851) \times 3.25\%}{1 - \frac{1}{(1+3.25\%)^{20}}}$$
$$= \$386478.204/\text{year}$$

3.4 Calculation of operating costs

Commonly, the operation duration is 8000 hrs for each year, and the rest is used for equipment maintenance. Consequently, we simulate the energy consumption of various operations including heat exchanger, pump and compressor. The running results of operation cost are shown in Table S9-S12. Specifically,

Assuming its price is 3 cents per kWh[8,9], the electricity cost is calculated according to the electricity demand and price:

$$\text{Electricity cost} = 25141.152 \text{ kW} \times \frac{\$0.03}{\text{kWh}} \times 8000 \frac{\text{h}}{\text{year}} = \$6033876.48/\text{year}$$

The maintenance cost is assumed 2.5% of capital cost per year (from H2A):

$$\text{Maintenance cost} = \$386478.204 \text{ /year} \times 2.5\% = \$9661.955/\text{year}$$

Given the industrial O_2 price set to be about $< \$0.1/\text{kg}$ (source: https://www.intratec.us/chemical-markets/oxygen-price), the total cost of O_2 is:

$$O_2 \text{ cost} = 2962 \text{ kg/hr} \times \$0.1/\text{kg} \times 8000 \text{ hr/year} = \$2369600/\text{year}$$

The industrial water is about $\$0.00191/\text{gallon}$ or $\$0.0005046/\text{kg}$ (https://www.fbgtx.org/673/Industrial-Water-Rates). The cost of water is:

$$H_2O \text{ cost} = 3522 \text{ kg/hr} \times \$0.0005046/\text{kg} \times 8000 \text{ hr/year} = \$14217.610 \text{ /year}$$

The operating cost of membrane separation is:

$$\text{Separation cost} = \$4124578.851 \times 10\% \text{ /year} = \$412457.8851 \text{ /year}$$

According to the average wage of the American manufacturing industry, it is estimated that the labor cost in the first year will be $500000, and the annual wage will increase by 5%. Therefore, the total labor cost for 20 years is $16532977.05.

The cost price of H2O2 is (Table S10):

The cost price of H_2O_2

$$= \frac{\left(\frac{\$386478.204}{\text{year}} + \frac{\$6033876.48}{\text{year}} + \frac{\$9661.955}{\text{year}} + \frac{\$2369600}{\text{year}} + \frac{\$14217.610}{\text{year}} + \frac{\$412457.8851}{\text{year}}\right) \times 20 \text{ year} + \$16532977.05}{\frac{4463\text{kg}}{\text{h}} \times 70\% \times \frac{8000\text{h}}{\text{year}} \times 20 \text{ year}}$$

$$= \$0.40 \text{ kg}^{-1}$$

The is given by the product revenue minus operating costs, and 25% tax. The market price of 70 wt% H2O2 is reported as $0.556/kg.

First $-$ year profit

$$
\begin{aligned}
= \Bigg(&\frac{4463\text{kg}}{\text{h}} \times \frac{\$0.556}{\text{kg}} \times \frac{8000\text{h}}{\text{year}} - \frac{\$386478.204}{\text{year}} - \frac{\$6033876.48}{\text{year}} \\
&- \frac{\$9661.955}{\text{year}} - \frac{\$2369600}{\text{year}} - \frac{\$14217.610}{\text{year}} - \frac{\$412457.8851}{\text{year}} \\
&- \$500000 \Bigg) \times (1 - 25\%) = \$7593848.899
\end{aligned}
$$

Finally, the payback time should be:

$$
\text{payback time} = \frac{\$386478.204 \times 20}{\$7593848.899/\text{year}} = 1 \text{ year}
$$

In addition, The FNPV is analyzed, indicating that the scheme is feasible and the investment benefit is good (Table S11).

$$
\text{FNPV} = \sum_{t=0}^{n} (Cl - CO)_t \times (1 + i)^{-t}
$$

Where Cl is the present value of future cash flow, CO is the present value of the original investment, i is the discount rate, and t is the duration.

In addition, our on-site power generation method does not require transportation and storage costs. In contrast, the H_2O_2 cost of the traditional industrial anthraquinone production process without transportation and storage cost is about $1.5/kg (http://www.h2o2.com/faqs/FaqDetail.aspx?fId=25). Therefore, we can conclude that our strategy is competitive with the current anthraquinone method for H_2O_2 production.

II. Supplementary Results
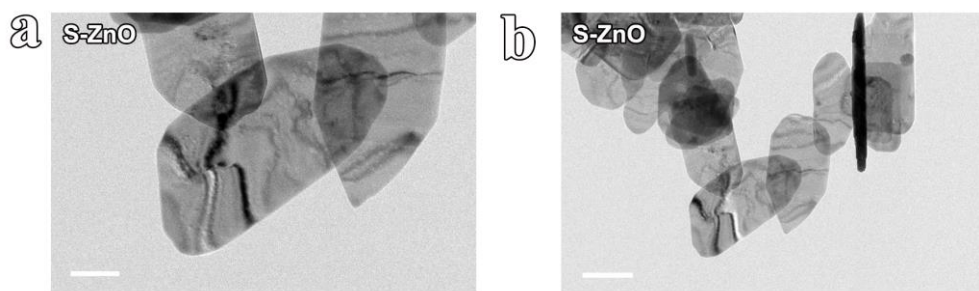
Fig. S1 Transmission electron microscopy (TEM) images of S-ZnO crystal (scale bar: 100 nm for a; 200 nm for b).
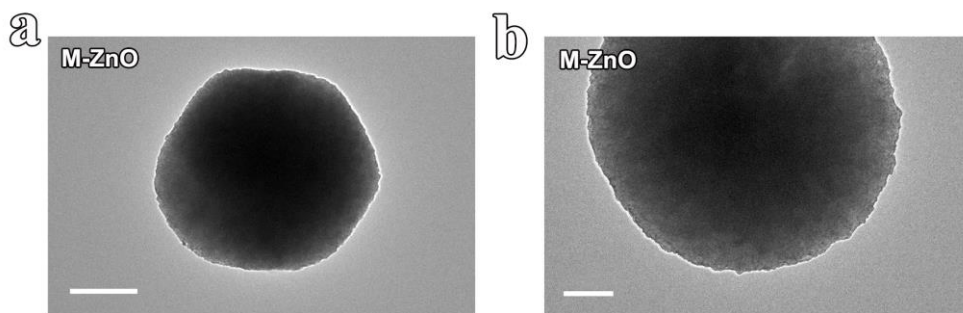
Fig. S2 Transmission electron microscopy (TEM) images of M-ZnO crystal (scale bar: 500 nm for a; 200 nm for b).
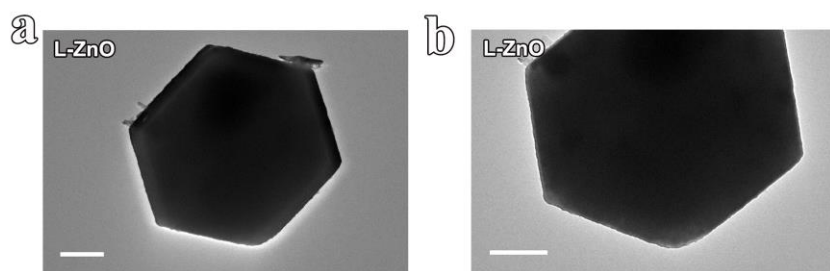
Fig. S3 Transmission electron microscopy (TEM) images of L-ZnO crystal (scale bar: 500 nm for a, b).
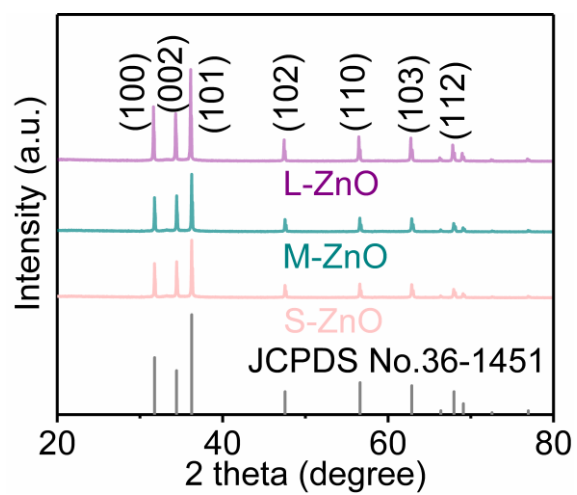
Fig. S4 XRD patterns of S-, M- and L-ZnO crystals.
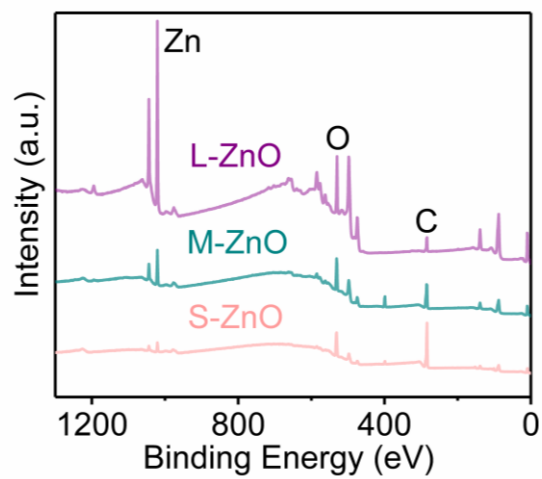
Fig. S5 X-ray photoelectron spectroscopy (XPS) survey of S-, M- and L-ZnO crystals.
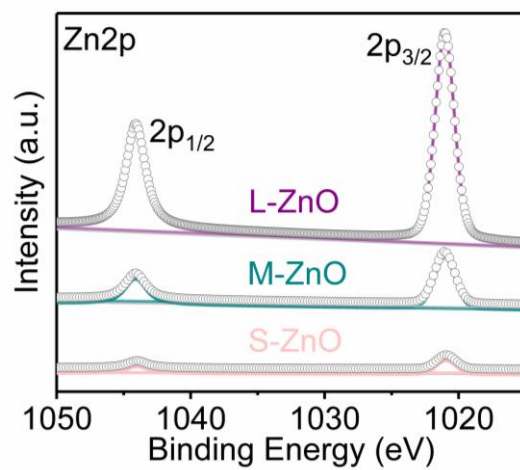
Fig. S6 X-ray photoelectron spectroscopy (XPS) Zn 2p spectra of S-, M- and L-ZnO crystals.
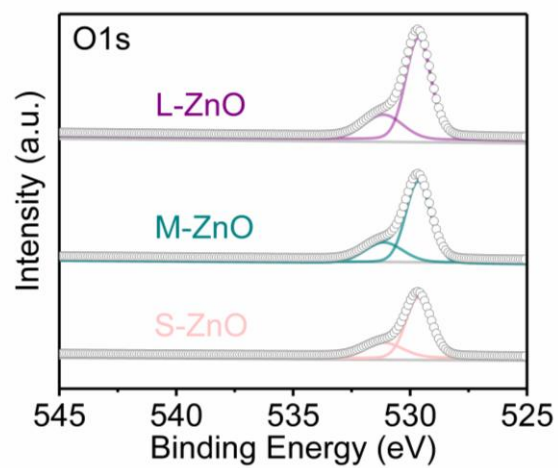
Fig. S7 X-ray photoelectron spectroscopy (XPS) O 1s spectra of S-, M- and L-ZnO crystals.
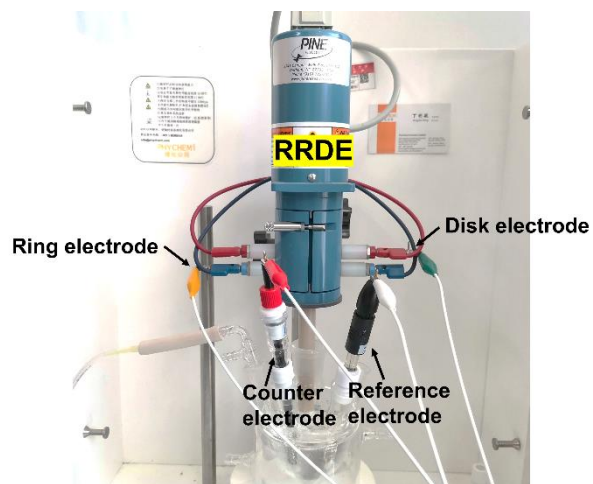
Fig. S8 Optical image of rotating ring-disk electrode (RRDE) setup.
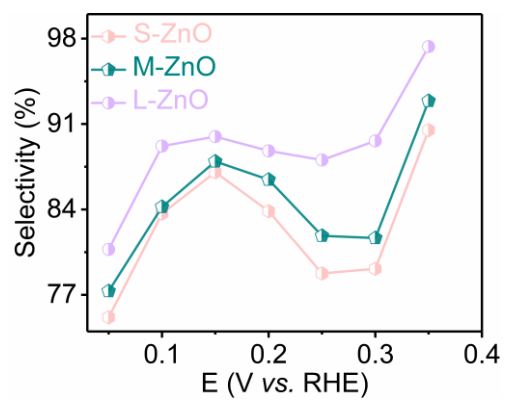
Fig. S9 The H$_2$O$_2$ molar selectivity of S-, M- and L-ZnO evaluated by RRDE.
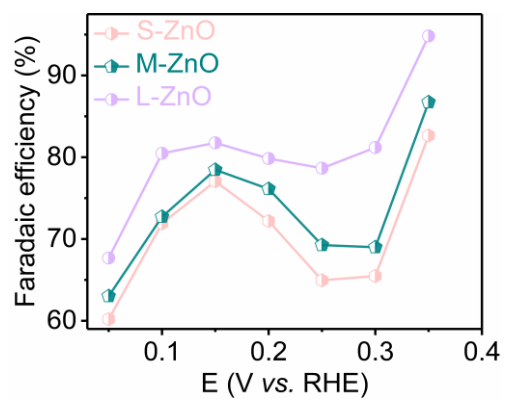
Fig. S10 The H$_2$O$_2$ Faradaic efficiencies (FE) of S-, M- and L-ZnO evaluated by RRDE.
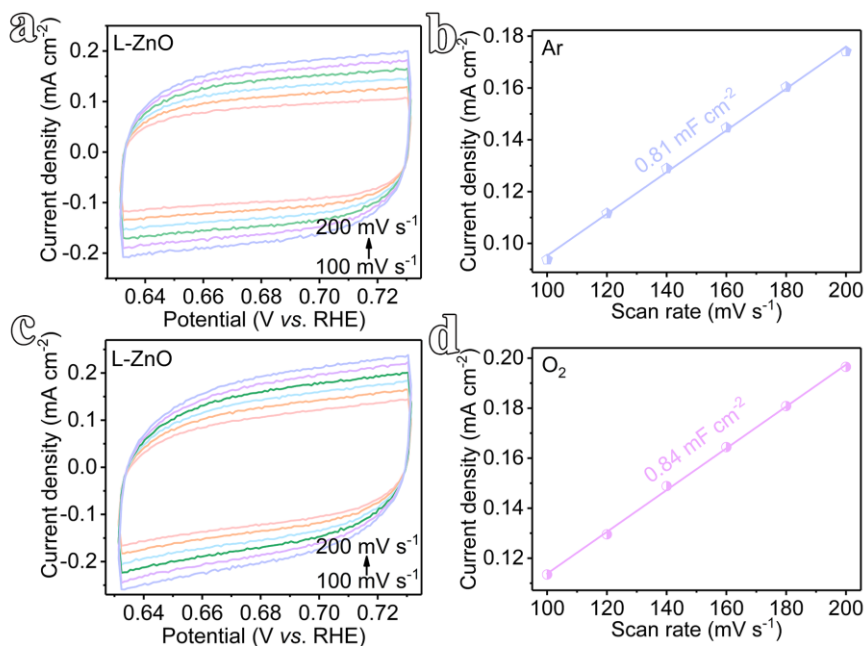
Fig. S11 Electric double layer capacitances of L-ZnO electrode in Ar- and O$_2$-saturated 0.6 M K$_2$SO$_4$ electrolytes. (a, c) CVs measured at different scan rates from 100 to 200 mV s^{-1} at the potential range of 0.631~0.731 V (*vs.* RHE); (b, d) the corresponding current densities at 0.681 V (*vs.* RHE) plotted against scan rates.

Supplementary note.

The capacitances of L-ZnO electrode under Ar- and O$_2$-saturated 0.6 M K$_2$SO$_4$ were evaluated on the basis of CVs. The CVs of L-ZnO in Ar and O$_2$ display analogous rectangular shape of electrical double layer capacitor at the potential range of 0.631-0.731 V (*vs.* RHE). The plots of current density against scan rate show the linear relationship, and the slopes are the double layer capacitances. The values of double layer capacitances are 0.81 and 0.84 mF cm^{-2} for L-ZnO electrode under Ar and O$_2$, respectively.
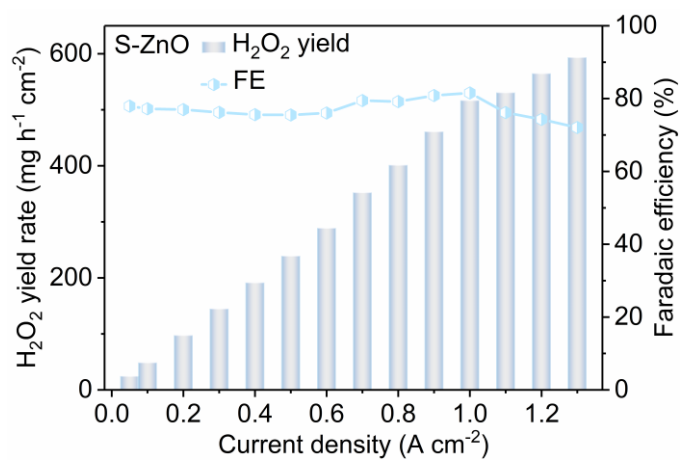
Fig. S12 The H₂O₂ yield rates and Faradaic efficiencies (FE) of S-ZnO calculated by chronopotentiometry test in flow-type cell.
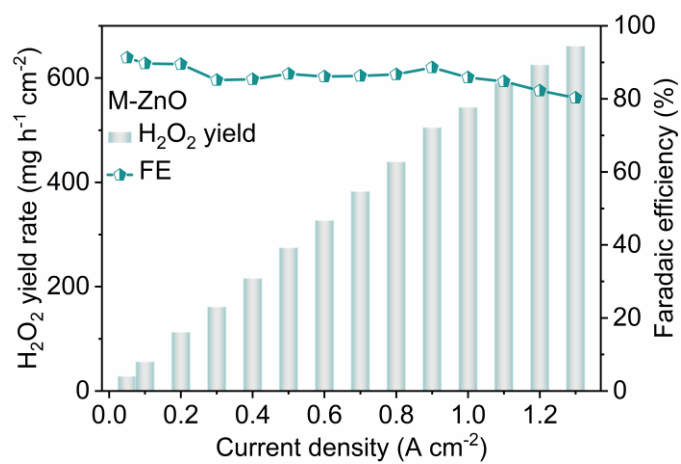
Fig. S13 The H_2O_2 yield rates and Faradaic efficiencies (FE) of M-ZnO calculated by chronopotentiometry test in flow-type cell.
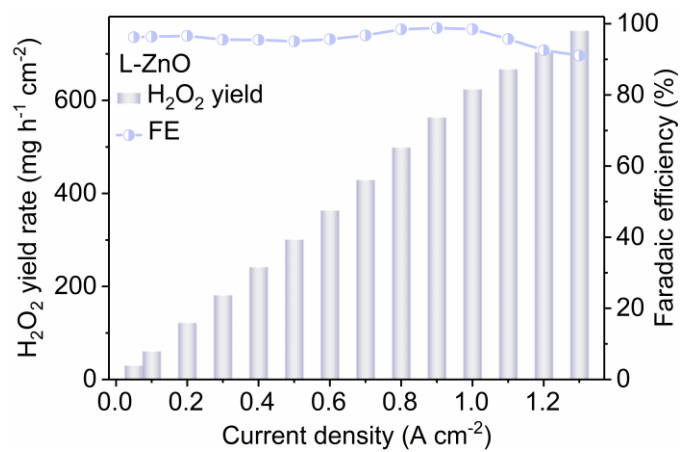
Fig. S14 The H₂O₂ yield rates and Faradaic efficiencies (FE) of L-ZnO calculated by chronopotentiometry test in flow-type cell.
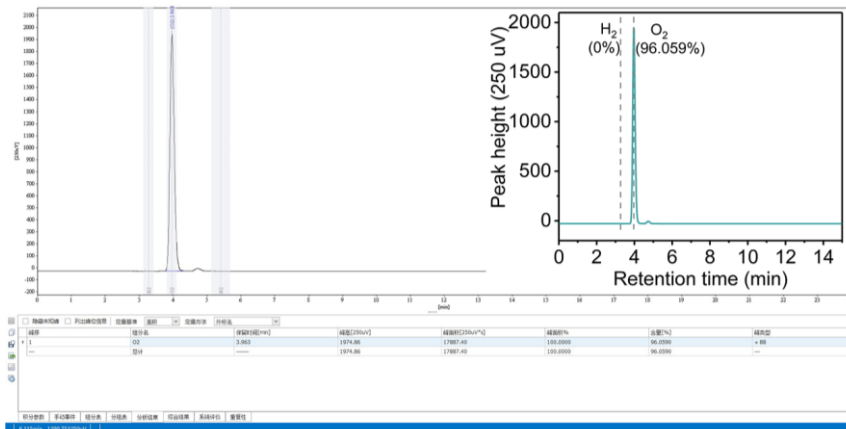
Fig. S15 The gas chromatography (GC) analyses of gaseous products collected from chronopotentiometric ORR test of L-ZnO electrode at 1 A cm^{-2}.
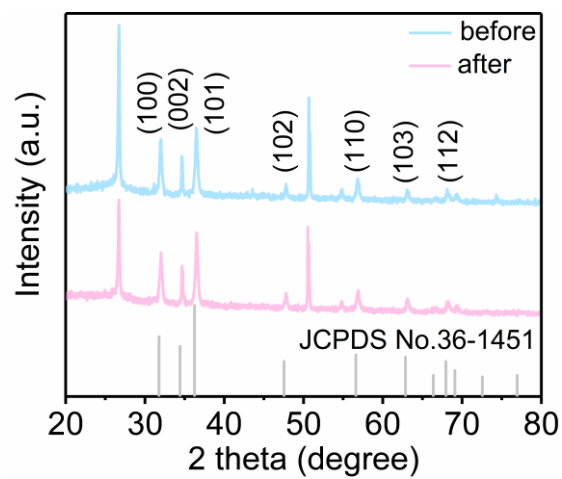
Fig. S16 The XRD patterns of L-ZnO electrode before and after chronopotentiometry tests at 1 A cm^{-2}.
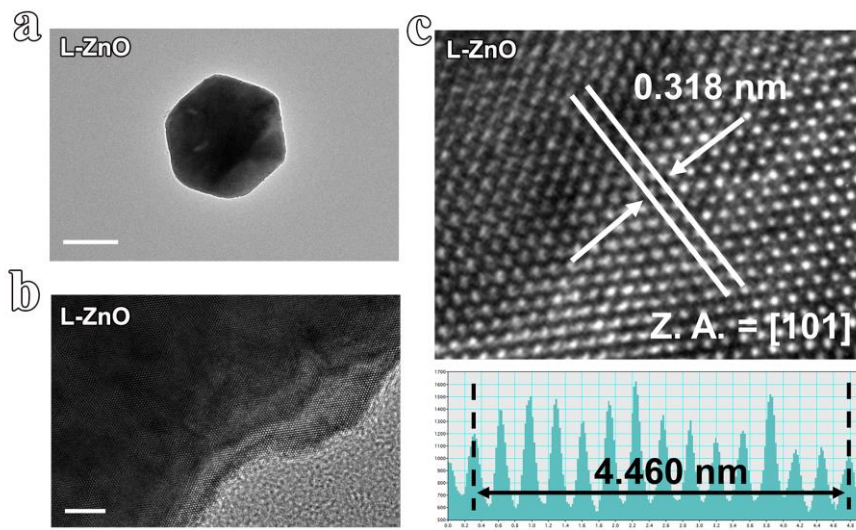
Fig. S17 The morphological characterizations of L-ZnO electrode after chronopotentiometry test at 1 A cm^{-2}. (a) Transmission electron microscopy (TEM) image (scale bar: 500 nm); (b) High-resolution transmission electron microscopy (HRTEM) image (scale bar: 5 nm); (c) Lattice spacing showing in HRTEM image.
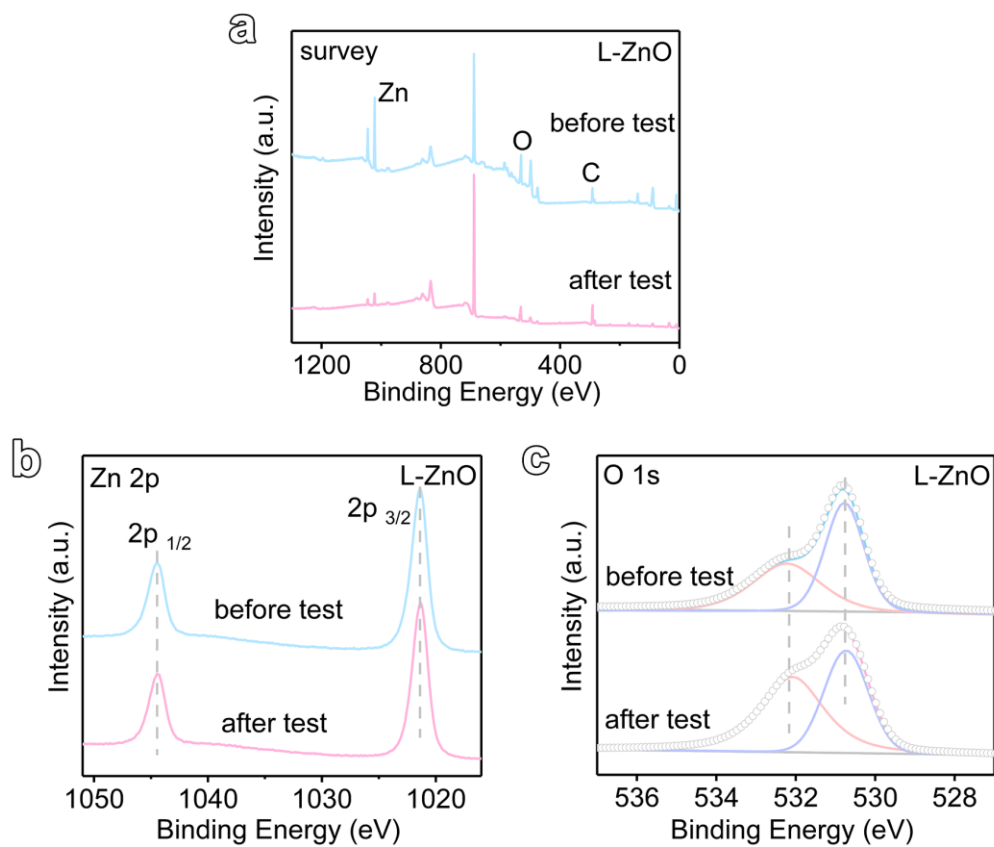
Fig. S18 The X-ray photoelectron spectra (XPS) of L-ZnO electrode before and after chronopotentiometry tests at 1 A cm^{-2}. (a) overall survey; (b) Zn 2p; (c) O 1s.
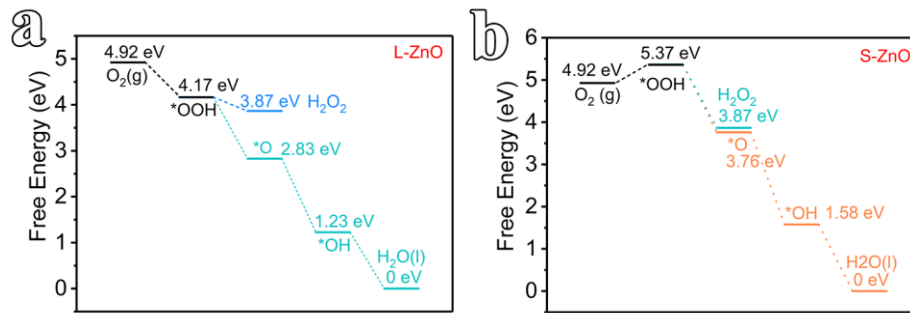
Fig. S19 The comparison of Gibbs free energy changes of L-ZnO (a) and S-ZnO (b).
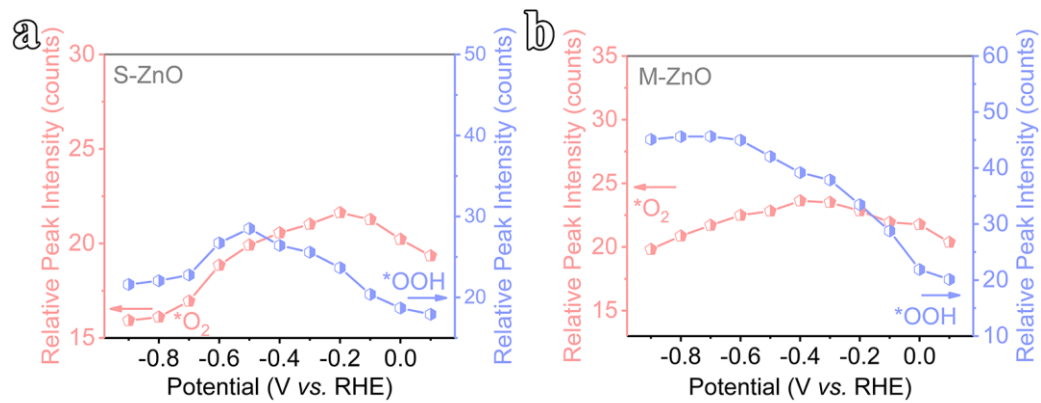
Fig. S20 The relative peak intensities of *O$_2$ and *OOH as a function of potentials for S- and M-ZnO.
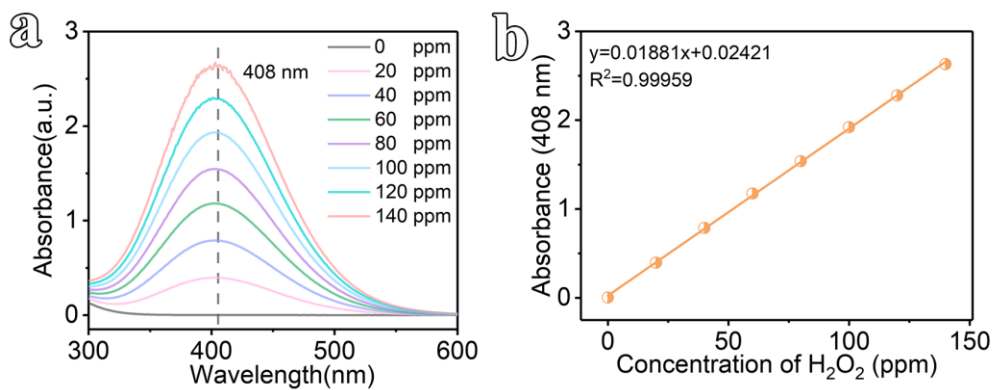
Fig. S21 Calibration curve for hydrogen peroxide measured by a traditional titration method in 0.6 M K_2SO_4 electrolyte. (a) The standard UV-Vis adsorption spectra of H_2TiO_4 with different H_2O_2 concentrations; (b) Calibration curve used for estimation of H_2O_2 concentrations.
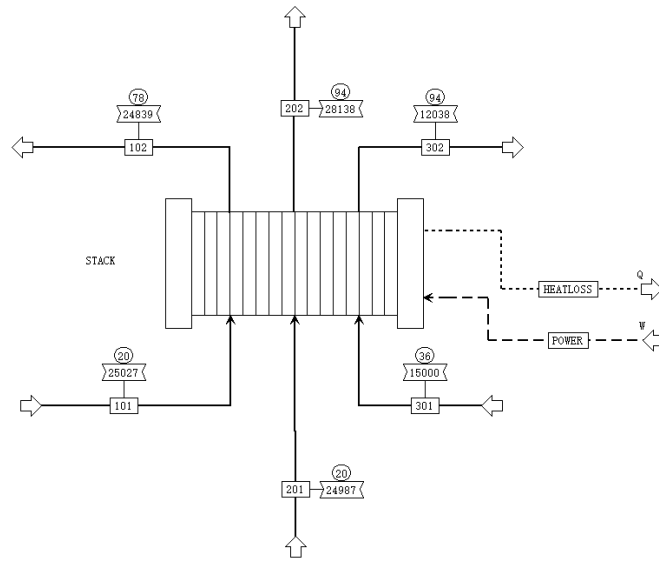
Fig. S22 Model of ACM electrolysis.
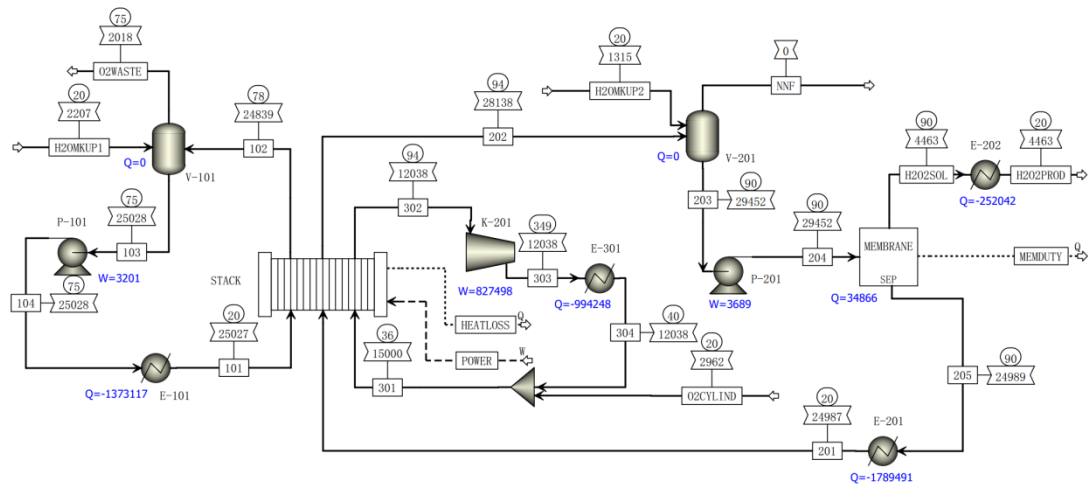
Fig. S23 Flowsheet of the process simulations for H_2O_2 production.
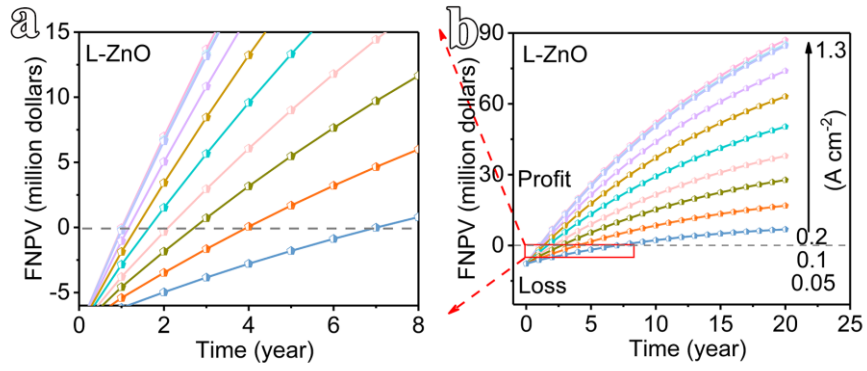
Fig. S24 FNPV analysis for L-ZnO at different current densities.
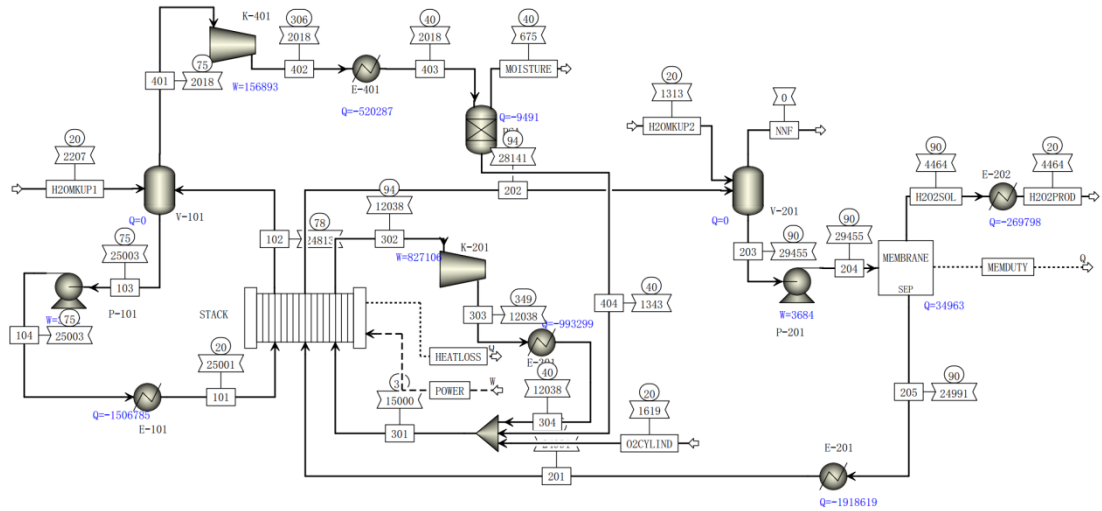
Fig. S25 Schematic diagram of Route 2 (the circulation of oxygen produced by the anode to cathode by using molecular sieve).

Table S1. The comparison of Faradaic efficiencies (FE) of different ZnO samples in 0.6 M K_2SO_4 electrolyte.

Current densities (A cm^{-2})	L-ZnO (%)	M-ZnO (%)	S-ZnO (%)
0.05	96.23	91.28	77.96
0.1	96.38	89.71	77.22
0.2	96.62	89.52	76.99
0.3	95.54	85.16	76.21
0.4	95.48	85.37	75.60
0.5	95.08	86.85	75.51
0.6	95.66	86.12	76.04
0.7	96.76	86.31	79.46
0.8	98.46	86.72	79.19
0.9	98.84	88.62	80.86
1.0	98.48	85.85	81.56
1.1	95.72	84.78	76.16
1.2	92.56	82.27	74.31
1.3	91.06	80.30	72.07

Table S2. The comparison of H_2O_2 yield rates of ZnO samples in 0.6 M K_2SO_4 electrolyte.

Current densities (A cm⁻²)	L-ZnO (mg h⁻¹ cm⁻²)	M-ZnO (mg h⁻¹ cm⁻²)	S-ZnO (mg h⁻¹ cm⁻²)
0.05	30.50	28.93	24.71
0.1	61.09	56.86	48.94
0.2	122.48	113.47	97.59
0.3	181.68	161.92	144.92
0.4	242.07	216.44	191.68
0.5	301.32	275.24	239.29
0.6	363.76	327.52	289.15
0.7	429.32	382.92	352.54
0.8	499.23	439.68	401.51
0.9	563.78	505.53	461.24
1.0	624.15	544.15	516.96
1.1	667.36	591.05	530.98
1.2	704.02	625.69	565.11
1.3	750.29	661.70	593.84

Table S3. The comparison of ZnO samples with the state-of-the art electrocatalysts.

Catalyst	Electrolyte	H_2O_2 yield (mg cm^{-2} h^{-1})	Faradaic efficiency (%)	j (mA cm^{-2})	References
L-ZnO	0.6 M K$_2$SO$_4$	624.15	98.48	1000	This work
B-C[10]	1 M Na$_2$SO$_4$	N/A	83.2	300	*Nat. Commun.* 2021, **12**, 4225
Natural air diffusion electrode (NADE)[11]	0.05 M Na$_2$SO$_4$	101.67	66.8	240	*Nat. Commun.* 2020, **11**, 1731
Co SACs[12]	0.5 M NaCl (O$_2$)	47.813	95.6	50	*Energy Environ. Sci.* 2021, **14**, 5444-5456
Co SACs[12]	0.5 M NaCl (air)	36.125	72.4	50	*Energy Environ. Sci.* 2021, **14**, 5444-5456
N-doped mesoporous carbon (N-doped CMK-3)[13]	0.1 M K$_2$SO$_4$	18.601	> 70	3.0 in RRDE	*ACS Catal.* 2018, **8**, 2844-2856
N-doped carbon nanohorns (g-N-CNHs)[14]	0.1 M PBS	1.428	~ 90	~ 0.5 in RRDE	*Chem* 2018, **4**, 106-123
O-CNTs[15]	0.1 M PBS	N/A	~ 85	~ 1.62 in RRDE	*Nat. Catal.* 2018, **1**, 156-162
a-PdSe$_2$ NPs/C[16]	0.1 M Na$_2$SO$_4$	17.3088	96.3	50	*Adv. Mater.* 2023, **35**, 2208101
Ni$_3$HAB$_2$[17]	0.05 M NaPi	13.24	73	8.0	*J. Am. Chem. Soc.* 2022, **144**, 15845-15854
CoPc-OCNT[18]	0.3 M K$_2$SO$_4$	195.959	96	300	*Nat. Commun.* 2023, **14**, 172
Ni$_{2-x}$P-V$_{Ni}$[19]	0.1 M PBS	1.3158	91.5	14.91	*Adv. Mater.* 2022, **34**, 2106541
Co-rPB-1 (6)[20]	0.1 M PBS	N/A	> 90	1.0	*Angew. Chem. Int.*

					Ed. 2020, **59**, 4902-4907
Fe-CNT[21]	0.1 M PBS	6.913	> 80	20	*Nat. Commun.* 2019, **10**, 3997
MCHS[22]	0.1 M PBS	N/A	> 90	3.0 in RRDE	*ACS Catal.* 2020, **10**, 7434-7442
Pd$_{17}$Se$_{15}$Pd$_3$ B[23]	0.1 M KPi	N/A	~ 90	-5.0	*Applied Catalysis B: Environmental* 2022, **309**, 121265
O-C (Al)[24]	0.5 M Na$_2$SO$_4$	17.34	~ 92	30	*Nat. Commun.* 2020, **11**, 5478

Table S4. The inductively coupled plasma mass spectroscopy (ICP-MS) analysis of Zn percentages in L-ZnO before and after chronopotentiometry test at the current density of 1 A cm^{-2}.

Test element	Test solution element concentrations (μg L^{-1})	Dilution ratios	Elemental concentrations of the original solution of the digestion (μg L^{-1})	Sample element contents (%)
Before test	170.616	10000	1706163	73.54
After test	117.839	10000	1178392	72.03

Table S5. The comparison of the adsorption energies of *OOH between L-/S-ZnO.

Entry	Total Energy (eV)	Energy of *OOH (eV)	Energy of substrate (eV)	Adsorption energy (eV)
L-ZnO + *OOH	-693.1908	-13.8559	-678.8265	-0.5084
S-ZnO + *OOH	-280.2802	-13.8559	-267.1229	0.6983

Table S6. The comparison of the adsorption energies of *O between L- and S-ZnO.

Entry	Total Energy (eV)	Energy of *O (eV)	Energy of substrate (eV)	Adsorption energy (eV)
L-ZnO + *O	-683.4017	-3.9190	-678.8265	0.6562
S-ZnO + *O	-271.1171	-3.9190	-267.122911	-0.0752

Table S7. The comparison of the formation energies of *OOH and *O between L- and S-ZnO.

Entry	+ *OOH	+ *O
L-ZnO	-0.5084	0.6562
S-ZnO	0.6983	-0.0752

Table S8. The input of streams for techno-economic assessment.

stream	Components	Temperature (°C)	Pressure (atm)	Flow (kg/hr)
Anode	0.6 M K_2SO_4	20	1	25000
Cathode	0.6 M K_2SO_4	20	1	25000
Gas	0.6 M K_2SO_4	25	1	15000

Table S9. Simulated data of L-, M- and S-ZnO for techno-economic assessment.

Current densities (A cm^{-2})	Potential (V)	material	FE (%)	H$_2$O$_2$ production (70wt %, kg/hr)	H$_2$O consumption of anode (kg/h)	H$_2$O consumption of cathode (kg/h)	O$_2$ consumption of cathode (kg/h)	Electrolytic power (kW)	Current (A)	Electrolytic area (m^2)	Anode cycle power (kW)	Cathode cycle power (kW)	O$_2$ cycle power (kW)	Electrolyte cooling power of Anode (kW)	Electrolyte cooling power of cathode (kW)	Cooling power of H2O2 (kW)	Cooling power of O$_2$ (kW)	Membrane separation power (kW)
-0.05	-2.0847	L-ZnO	96.23	218	84	63	146	521.175	250000	500	3.071	3.091	843.881	106.815	108.22	0.742	801.81	1.866
-0.1	-2.2798	L-ZnO	96.38	437	174	125	293	1139.9	500000	500	3.089	3.13	853.893	284.927	289.248	3.974	837.587	3.732
-0.2	-2.6026	L-ZnO	96.62	876	359	251	587	2602.6	1000000	500	3.126	3.215	874.363	647.605	667.049	18.365	910.463	7.449
-0.3	-2.875	L-ZnO	95.55	1298	564	366	876	4312.5	1500000	500	3.156	3.289	889.594	949.895	1001.722	40.875	970.659	11.007
-0.4	-3.1611	L-ZnO	95.48	1731	802	489	1167	6322.2	2000000	500	3.18	3.361	896.907	1163.27	1268.538	69.051	1012.289	14.536
-0.5	-3.2386	L-ZnO	95.08	2157	1042	608	1456	8096.5	2500000	500	3.193	3.418	892.72	1259.995	1419.209	96.403	1026.145	17.881
-0.6	-3.4858	L-ZnO	95.66	2596	1293	732	1752	10457.4	3000000	500	3.195	3.475	886.177	1328.793	1555.485	127.098	1035.005	21.462
-0.7	-3.5898	L-ZnO	96.76	3070	1531	883	2056	12564.3	3500000	500	3.206	3.53	873.617	1358.771	1633.759	158.006	1029.976	24.938
-0.8	-3.7195	L-ZnO	98.46	3564	1762	1044	2369	14878	4000000	500	3.198	3.586	858.653	1367.177	1695.505	190.242	1020.026	28.701
-0.9	-3.9041	L-ZnO	98.84	4029	1992	1188	2671	17568.45	4500000	500	3.202	3.637	843.606	1376.037	1750.549	222.063	1008.83	31.987
-1	-3.9726	L-ZnO	98.48	4463	2207	1315	2962	19863	5000000	500	3.201	3.689	827.498	1373.117	1789.491	252.042	994.248	34.866
-1.1	-4.4653	L-ZnO	95.72	4769	2452	1349	3212	24559.15	5500000	500	3.204	3.728	816.91	1388.411	1871.355	280.805	989.636	37.16
-1.2	-4.7117	L-ZnO	92.56	5035	2691	1360	3449	28270.2	6000000	500	3.205	3.764	806.655	1398.618	1948.391	308.769	984.554	38.916
-1.3	-4.9874	L-ZnO	91.06	5359	2986	1408	3707	32418.1	6500000	500	3.209	3.81	799.763	1434.679	2089.098	352.635	989.557	41.26
-0.05	-2.0292	M-ZnO	91.28	207	87	55	143	507.3	250000	500	3.071	3.09	843.825	104.196	105.684	0.687	801.376	1.773
-0.1	-2.3105	M-ZnO	89.71	406	172	104	283	1155.25	500000	500	3.094	3.128	855.581	296.339	300.651	3.834	840.8	3.488
-0.2	-2.7033	M-ZnO	89.52	812	360	209	566	2703.3	1000000	500	3.129	3.208	879.335	683.508	704.821	18	920.619	6.923
-0.3	-3.0214	M-ZnO	85.16	1157	571	274	829	4532.1	1500000	500	3.162	3.284	897.726	998.742	1060.838	38.574	986.337	9.859
-0.4	-3.1435	M-ZnO	85.37	1545	804	364	1107	6287	2000000	500	3.18	3.342	901.331	1167.65	1280.448	62.25	1017.933	13.095

-0.5	-3.3483	M-ZnO	86.85	1972	1050	484	1394	8370.75	2500000	500	3.192	3.401	899.275	1278.566	1452.949	90.366	1036.838	16.407
-0.6	-3.5889	M-ZnO	86.12	2345	1304	566	1667	10766.7	3000000	500	3.199	3.455	893.608	1342.797	1586.424	117.218	1045.819	19.373
-0.7	-3.8198	M-ZnO	86.31	2738	1547	661	1946	13369.3	3500000	500	3.203	3.505	883.576	1374.126	1680.112	144.781	1044.917	22.484
-0.8	-3.9991	M-ZnO	86.72	3141	1780	762	2229	15996.4	4000000	500	3.204	3.553	870.571	1384.951	1745.169	172.487	1037.118	25.577
-0.9	-4.1885	M-ZnO	88.62	3616	2006	914	2533	18848.25	4500000	500	3.204	3.608	854.927	1388.675	1796.713	204.307	1024.724	28.989
-1	-4.3853	M-ZnO	85.85	3890	2231	928	2774	21926.5	5000000	500	3.209	3.637	842.955	1391.722	1847.865	226.421	1015.863	31.001
-1.1	-4.6821	M-ZnO	84.78	4228	2463	988	3033	25751.55	5500000	500	3.205	3.682	832.51	1395.156	1914.378	254.657	1007.507	33.374
-1.2	-4.9346	M-ZnO	82.27	4485	2712	994	3264	29607.6	6000000	500	3.209	3.711	821.71	1411.754	2000.997	283.291	1005.559	35.011
-1.3	-5.2708	M-ZnO	80.3	4722	3112	1230	3498	34260.2	6500000	500	3.215	3.754	826.061	1489.721	2121.708	315.218	1035.8	37.027
-0.05	-2.0335	S-ZnO	77.96	177	87	35	133	508.375	250000	500	3.071	3.088	845.062	110.782	112.514	0.625	803.514	1.514
-0.1	-2.3123	S-ZnO	77.22	350	174	67	264	1156.15	500000	500	3.091	3.124	857.726	306.227	311.946	3.434	844.397	2.998
-0.2	-2.5679	S-ZnO	76.99	698	357	132	528	2567.9	1000000	500	3.127	3.195	879.454	662.455	685.543	15.054	917.839	5.974
-0.3	-2.8319	S-ZnO	76.21	1035	569	190	789	4247.85	1500000	500	3.155	3.259	896.313	960.826	1020.502	33.299	979.643	8.852
-0.4	-3.0432	S-ZnO	75.6	1371	801	248	1048	6086.4	2000000	500	3.179	3.323	903.758	1156.013	1272.115	54.96	1018.945	11.617
-0.5	-3.2396	S-ZnO	75.51	1711	1048	307	1310	8099	2500000	500	3.191	3.374	903.634	1268.977	1450.668	78.218	1040.313	14.422
-0.6	-3.4505	S-ZnO	76.04	2065	1295	376	1576	10351.5	3000000	500	3.198	3.425	898.144	1331.736	1581.871	102.898	1049.248	17.309
-0.7	-3.7094	S-ZnO	79.46	2521	1541	516	1875	12982.9	3500000	500	3.203	3.482	887.356	1367.322	1677.614	133.178	1048.077	20.826
-0.8	-4.0076	S-ZnO	79.19	2870	1781	580	2139	16030.4	4000000	500	3.204	3.529	876.713	1384.994	1759.514	158.845	1044.453	23.528
-0.9	-4.2973	S-ZnO	80.86	3291	2012	691	2429	19337.85	4500000	500	3.205	3.568	862.661	1392.372	1813.884	188.214	1034.71	26.793
-1	-4.4761	S-ZnO	81.56	3700	2235	802	2710	22380.5	5000000	500	3.205	3.625	847.814	1391.664	1866.347	217.11	1022.258	29.588
-1.1	-4.7448	S-ZnO	76.16	3796	2463	699	2892	26096.4	5500000	500	3.208	3.639	840.356	1397.321	1935.674	231.331	1019.481	30.376
-1.2	-5.1278	S-ZnO	74.31	4038	2736	693	3122	30766.8	6000000	500	3.208	3.679	834.257	1424.035	2062.404	262.12	1022.991	32.195
-1.3	-5.4198	S-ZnO	72.07	4237	3408	1477	3338	35228.7	6500000	500	3.226	3.705	862.246	1587.34	2115.716	282.262	1110.322	33.557

Table S10. H_2O_2 production costs under various current densities.

Current density (A cm^{-2})	Material	Equipment cost ($)	Electricity cost ($)	O$_2$ cost ($)	H$_2$O cost ($)	Maintenance cost ($)	Separation cost ($)	Labor cost ($)	Total cost ($)	70 wt% H$_2$O$_2$ production (kg)	H$_2$O$_2$ production (kg)	H$_2$O$_2$ average cost ($/kg)
0.05	L-ZnO	7729564.085	11475220.8	2336000	11868.192	193239.1021	8249357.703	16532977.05	46528226.93	34880000	24416000	1.905644943
0.1	L-ZnO	7729564.085	16413504	4688000	24140.064	193239.1021	8249357.703	16532977.05	53830782.01	69920000	48944000	1.099844353
0.2	L-ZnO	7729564.085	27524328	9392000	49248.96	193239.1021	8249357.703	16532977.05	69670714.9	140160000	98112000	0.710114103
0.3	L-ZnO	7729564.085	39276945.6	14016000	75084.48	193239.1021	8249357.703	16532977.05	86073168.02	207680000	145376000	0.592072749
0.4	L-ZnO	7729564.085	51615993.6	18672000	104230.176	193239.1021	8249357.703	16532977.05	103097361.7	276960000	193872000	0.531780565
0.5	L-ZnO	7729564.085	61514227.2	23296000	133214.4	193239.1021	8249357.703	16532977.05	117648579.5	345120000	241584000	0.486988292
0.6	L-ZnO	7729564.085	74006832	28032000	163490.4	193239.1021	8249357.703	16532977.05	134907460.3	415360000	290752000	0.463994952
0.7	L-ZnO	7729564.085	84720494.4	32896000	194896.704	193239.1021	8249357.703	16532977.05	150516529	491200000	343840000	0.437751655
0.8	L-ZnO	7729564.085	96216422.4	37904000	226545.216	193239.1021	8249357.703	16532977.05	167052105.6	570240000	399168000	0.418500745
0.9	L-ZnO	7729564.085	109480132.8	42736000	256740.48	193239.1021	8249357.703	16532977.05	185178011.2	644640000	451248000	0.410368603
1	L-ZnO	7729564.085	120677529.6	47392000	285078.816	193239.1021	8249357.703	16532977.05	201059746.4	714080000	499856000	0.402235336
1.1	L-ZnO	7729564.085	143761723.2	51392000	306877.536	193239.1021	8249357.703	16532977.05	228165738.7	763040000	534128000	0.42717427
1.2	L-ZnO	7729564.085	162062745.6	55184000	327061.536	193239.1021	8249357.703	16532977.05	250278945.1	805600000	563920000	0.443819948
1.3	L-ZnO	7729564.085	183034132.8	59312000	354753.984	193239.1021	8249357.703	16532977.05	275406024.7	857440000	600208000	0.458850973
0.05	M-ZnO	7729564.085	11380809.6	2288000	11848.008	193239.1021	8249357.703	16532977.05	46385795.55	33120000	23184000	2.000767579
0.1	M-ZnO	7729564.085	16618392	4528000	22283.136	193239.1021	8249357.703	16532977.05	53873813.08	64960000	45472000	1.184768936
0.2	M-ZnO	7729564.085	28429646.4	9056000	45938.784	193239.1021	8249357.703	16532977.05	70236723.13	129920000	90944000	0.772307388
0.3	M-ZnO	7729564.085	40946985.6	13264000	68221.92	193239.1021	8249357.703	16532977.05	86984345.46	185120000	129584000	0.671258377
0.4	M-ZnO	7729564.085	51533899.2	17712000	94299.648	193239.1021	8249357.703	16532977.05	102045336.8	247200000	173040000	0.589721086
0.5	M-ZnO	7729564.085	63128371.2	22304000	123849.024	193239.1021	8249357.703	16532977.05	118261358.2	315520000	220864000	0.535448775
0.6	M-ZnO	7729564.085	75737246.4	26672000	150976.32	193239.1021	8249357.703	16532977.05	135265360.7	375200000	262640000	0.515021934
0.7	M-ZnO	7729564.085	88924819.2	31136000	178265.088	193239.1021	8249357.703	16532977.05	152944222.2	438080000	306656000	0.498748507
0.8	M-ZnO	7729564.085	101947344	35664000	205230.912	193239.1021	8249357.703	16532977.05	170521712.9	502560000	351792000	0.484723112

0.9	M-ZnO	7729564.085	115936305.6	40528000	235749.12	193239.1021	8249357.703	16532977.05	189405192.7	578560000	404992000	0.46767638
1.0	M-ZnO	7729564.085	130988030.4	44384000	255045.024	193239.1021	8249357.703	16532977.05	208332213.4	622400000	435680000	0.478177133
1.1	M-ZnO	7729564.085	149740891.2	48528000	278619.936	193239.1021	8249357.703	16532977.05	231252649.1	676480000	473536000	0.488352837
1.2	M-ZnO	7729564.085	168829641.6	52224000	299207.616	193239.1021	8249357.703	16532977.05	254057987.2	717600000	502320000	0.505769205
1.3	M-ZnO	7729564.085	192444979.2	55968000	350555.712	193239.1021	8249357.703	16532977.05	281468672.9	755520000	528864000	0.532213713
0.05	S-ZnO	7729564.085	11465016	2128000	9849.792	193239.1021	8249357.703	16532977.05	46308003.73	28320000	19824000	2.335956605
0.1	S-ZnO	7729564.085	16747646.4	4224000	19457.376	193239.1021	8249357.703	16532977.05	53696241.72	56000000	39200000	1.369802085
0.2	S-ZnO	7729564.085	27554596.8	8448000	39479.904	193239.1021	8249357.703	16532977.05	68747214.65	111680000	78176000	0.879390281
0.3	S-ZnO	7729564.085	39137755.2	12624000	61278.624	193239.1021	8249357.703	16532977.05	84528171.77	165600000	115920000	0.729194028
0.4	S-ZnO	7729564.085	50449488	16768000	84692.064	193239.1021	8249357.703	16532977.05	100007318	219360000	153552000	0.651292839
0.5	S-ZnO	7729564.085	61736625.6	20960000	109397.28	193239.1021	8249357.703	16532977.05	115511160.8	273760000	191632000	0.60277595
0.6	S-ZnO	7729564.085	73628779.2	25216000	134909.856	193239.1021	8249357.703	16532977.05	131684827	330400000	231280000	0.569374036
0.7	S-ZnO	7729564.085	86994998.4	30000000	166073.952	193239.1021	8249357.703	16532977.05	149866210.3	403360000	282352000	0.530777931
0.8	S-ZnO	7729564.085	102168864	34224000	190617.696	193239.1021	8249357.703	16532977.05	169288619.6	459200000	321440000	0.52665698
0.9	S-ZnO	7729564.085	118383633.6	38864000	218229.408	193239.1021	8249357.703	16532977.05	190171001	526560000	368592000	0.515939035
1.0	S-ZnO	7729564.085	133258132.8	43360000	245195.232	193239.1021	8249357.703	16532977.05	209568466	592000000	414400000	0.50571541
1.1	S-ZnO	7729564.085	151477372.8	46272000	255287.232	193239.1021	8249357.703	16532977.05	230709798	607360000	425152000	0.542652505
1.2	S-ZnO	7729564.085	174776107.2	49952000	276843.744	193239.1021	8249357.703	16532977.05	257710088.9	646080000	452256000	0.569832327
1.3	S-ZnO	7729564.085	197889955.2	53408000	394395.36	193239.1021	8249357.703	16532977.05	284397488.5	677920000	474544000	0.599306889

Table S11. FNPV ($) analysis of L-ZnO at different current densities.

J (A cm⁻²) Time (year)	1.3	1.2	1.1	-1	-0.9	-0.8	-0.7	-0.6	-0.5	-0.4	-0.3	-0.2	-0.1	-0.05
0	-7729564.085	-7729564.085	-7729564.085	-7729564.085	-7,729,564	-7,729,564	-7,729,564	-7,729,564	-7,729,564	-7,729,564	-7,729,564	-7,729,564	-7,729,564	-7,729,564
1	-43418.65779	-174594.3846	-229281.4577	-232612.924	-1,043,212	-1,872,049	-2,849,746	-3,797,041	-4,574,304	-5,406,998	-6,173,594	-6,927,475	-7,755,414	-8,189,847
2	6996802.699	6740697.708	6633927.708	6627423.417	5,044,826	3,426,621	1,517,782	-331,699	-1,849,211	-3,474,948	-4,971,636	-6,443,498	-8,059,950	-8,908,128
3	13684768.62	13309683.37	13153310.59	13143784.56	10,825,950	8,455,965	5,660,326	2,951,621	729,109	-1,651,907	-3,843,920	-5,999,574	-8,366,991	-9,609,212
4	20037253.16	19548853.4	19345239.86	19332835.99	16,314,775	13,228,811	9,588,600	6,061,585	3,167,645	67,316	-2,786,912	-5,593,796	-8,676,418	-10,293,918
5	26070231.64	25473913.28	25225308.56	25210163.88	21,525,221	17,757,371	13,312,806	9,006,449	5,473,053	1,687,665	-1,797,244	-5,224,348	-8,988,117	-10,963,026
6	31798918.63	31099820.66	30808367.18	30790612.21	26,470,544	22,053,278	16,842,662	11,794,074	7,651,673	3,213,847	-871,710	-4,889,499	-9,301,980	-11,617,279
7	37237804.2	36440820.88	36108559.06	36088318.1	31,163,369	26,127,612	20,187,422	14,431,949	9,709,543	4,650,347	-7,256	-4,587,603	-9,617,904	-12,257,383
8	42400688.41	41510480.95	41139354.05	41116745.48	35,615,719	29,990,923	23,355,902	16,927,203	11,652,412	6,001,435	799,027	-4,317,089	-9,935,791	-12,884,013
9	47300714.2	46321721.84	45913580.58	45888717.13	39,839,045	33,653,260	26,356,495	19,286,629	13,485,756	7,271,179	1,549,908	-4,076,463	-10,255,548	-13,497,810
10	51950398.61	50886849.21	50443456.18	50416445.24	43,844,254	37,124,194	29,197,195	21,516,695	15,214,792	8,463,453	2,248,027	-3,864,303	-10,577,084	-14,099,386
11	56361662.68	55217582.77	54740616.61	54711560.45	47641731.69	40412837.67	31885617.8	23623560.47	16844485.64	9581944.051	2895894.701	-3679252.431	-10900316.09	-14689321.7
12	60545859.76	59325084.11	58816143.56	58785139.55	51241370.4	43527872.73	34429013.28	25613092.09	18379568.16	10630167.28	3495904.975	-3520020.556	-11225162.95	-15268172.27
13	64513802.55	63219983.35	62680590.99	62647731.9	54652590.95	46477565.98	36834287.9	27490877.31	19824544.7	11611468.31	4050336.528	-3385377.95	-11551547.7	-15836465.

												3	1	34
14	68275788.88	66912404.39	66344010.31	66309384.47	57884365.62	49269790.85	39108018.82	29262237.38	21183706.04	12529033.92	4561359.776	3274153.706	-11879397.14	-16394703.63
15	71841626.21	70411989.06	69815974.29	69779665.83	60945239.45	51912045.83	41256470.04	30932240.17	22461138.61	13385899.13	5031041.781	3185232.653	-12208641.49	-16943365.94
16	75220654.95	73727920.04	73105599.85	73067688.9	63843350.59	54411472.34	43285607.26	32505712.22	23660734.25	14184954.43	5461351.174	-3117552.74	-12539214.35	-17482908.29
17	78421770.76	76868942.74	76221569.77	76182132.64	66586449.63	56774871.74	45201112.09	33987250.22	24786199.48	14928952.67	5854162.84	3070102.482	-12871052.44	-18013764.94
18	81453445.68	79843386.12	79172153.37	79131262.73	69181918.1	59008721.51	47008395.6	35381231.99	25841064.33	15620515.63	6211262.386	3041918.563	-13204095.53	-18536349.51
19	84323748.33	82659182.55	81965226.18	81922951.25	71636786.03	61119190.67	48712611.2	36691826.87	26828690.72	16262140.21	6534350.389	3032083.539	-13538286.22	-19051055.9
20	87040363.1	85323886.62	84608288.72	84564695.42	73957748.69	63112154.5	50318666.86	37923005.67	27752280.48	16856204.44	6825046.447	3039723.651	-13873569.87	-19558259.27

Table S12. FNPV ($) analysis of different routes of L-ZnO at 1 A cm^{-2}.

Route Time (year)	Route 1	Route 2	Route 3	Route 4
0	-7729564.085	-7729564.085	-29344318.75	-30174798.84
1	-232612.924	372,790	-17,527,788	-17,616,978
2	6627423.417	7,809,401	-7,289,063	-6,700,509
3	13143784.56	14,874,881	2,445,098	3,679,121
4	19332835.99	21,586,902	11,698,720	13,547,476
5	25210163.88	27,962,297	20,494,687	22,928,903
6	30790612.21	34,017,094	28,854,791	31,846,588
7	36088318.1	39,766,561	36,799,789	40,322,615
8	41116745.48	45,225,237	44,349,446	48,378,015
9	45888717.13	50,406,970	51,522,589	56,032,817
10	50416445.24	55,324,946	58,337,147	63,306,098
11	54711560.45	59,991,726	64,810,196	70,216,026
12	58785139.55	64,419,272	70,957,997	76,779,903
13	62647731.9	68,618,976	76,796,039	83,014,207
14	66309384.47	72,601,687	82,339,072	88,934,633
15	69779665.83	76,377,738	87,601,145	94,556,127
16	73067688.9	79,956,970	92,595,636	99,892,924
17	76182132.64	83,348,756	97,335,287	104,958,581
18	79131262.73	86,562,021	101,832,233	109,766,010
19	81922951.25	89,605,267	106,098,033	114,327,507
20	84564695.42	92,486,590	110,143,692	118,654,782

References

1   G. Kresse, J. Furthmuller, *Computational Materials Science*, 1996, **6**, 15-50.
2   Kresse Furthmuller, *Physical review. B, Condensed matter*, 1996, **54**, 11169-11186.
3   Perdew, Burke Ernzerhof, *Physical review letters*, 1996, **77**, 3865-3868.
4   Perdew, Burke Wang, *Physical review. B, Condensed matter*, 1996, **54**, 16533-16539.
5   Blochl, *Physical review. B, Condensed matter*, 1994, **50**, 17953-17979.
6   G. Kresse, D. Joubert, *Physical Review B (Condensed Matter)*, 1999, **59**, 1758-1775.
7   Y. Sun, B. Xia, S. Ding, L. Yu, S. Chen, J. Duan, *J. Mater. Chem. A*, 2021, **9**, 20040-20047.
8   S. Chu, Y. Cui, N. Liu, *Nat. Mater.* 2016, **16**, 16-22.
9   Z. Huang, R. G. Grim, J. A. Schaidle, L. Tao, *Energy Environ. Sci.*, 2021, **14**, 3664-3678.
10   Y. Xia, X. Zhao, C. Xia, Z. Y. Wu, P. Zhu, J. Y. T. Kim, X. Bai, G. Gao, Y. Hu, J. Zhong, Y. Liu, H. Wang, *Nat. Commun.*, 2021, **12**, 4225.
11   Q. Zhang, M. Zhou, G. Ren, Y. Li, Y. Li, X. Du, *Nat. Commun.*, 2020, **11**, 1731.
12   Q. Zhao, Y. Wang, W. H. Lai, F. Xiao, Y. Lyu, C. Liao, M. Shao, *Energy Environ. Sci.*, 2021, **14**, 5444-5456.
13   Y. Sun, I. Sinev, W. Ju, A. Bergmann, S. Dresp, S. Kühl, C. Spöri, H. Schmies, H. Wang, D. Bernsmeier, B. Paul, R. Schmack, R. Kraehnert, B. Roldan Cuenya, P. Strasser, *ACS Catal.*, 2018, **8**, 2844-2856.
14   D. Iglesias, A. Giuliani, M. Melchionna, S. Marchesan, A. Criado, L. Nasi, M. Bevilacqua, C. Tavagnacco, F. Vizza, M. Prato, P. Fornasiero, *Chem*, 2018, **4**, 106-123.
15   Z. Lu, G. Chen, S. Siahrostami, Z. Chen, K. Liu, J. Xie, L. Liao, T. Wu, D. Lin, Y. Liu, T. F. Jaramillo, J. K. Nørskov, Y. Cui, *Nat. Catal.*, 2018, **1**, 156-162.
16   Z. Yu, S. Lv, Q. Yao, N. Fang, Y. Xu, Q. Shao, C. W. Pao, J. F. Lee, G. Li, L. M. Yang, X. Huang, *Adv. Mater.*, 2023, **35**, e2208101.
17   R. D. Ross, H. Sheng, Y. Ding, A. N. Janes, D. Feng, J. R. Schmidt, C. U. Segre, S. Jin, *J. Am. Chem. Soc.*, 2022, **144**, 15845-15854.
18   P. Cao, X. Quan, X. Nie, K. Zhao, Y. Liu, S. Chen, H. Yu, J. G. Chen, *Nat. Commun.*, 2023, **14**, 172.
19   Z. Zhou, Y. Kong, H. Tan, Q. Huang, C. Wang, Z. Pei, H. Wang, Y. Liu, Y. Wang, S. Li, X. Liao, W. Yan, S. Zhao, *Adv. Mater.*, 2022, **34**, e2106541.
20   P. T. Smith, Y. Kim, B. P. Benke, K. Kim, C. J. Chang, *Angew. Chem. Int. Ed.*, 2020, **59**, 4902-4907.
21   K. Jiang, S. Back, A. J. Akey, C. Xia, Y. Hu, W. Liang, D. Schaak, E. Stavitski, J. K. Norskov, S. Siahrostami, H. Wang, *Nat. Commun.*, 2019, **10**, 3997.
22   Y. Pang, K. Wang, H. Xie, Y. Sun, M. M. Titirici, G. L. Chai, *ACS Catal.*, 2020, **10**, 7434-7442.
23   J. Lee, S. W. Choi, S. Back, H. Jang, Y. J. Sa, *Applied Catalysis B:Environmental*, 2022, **309**, 121265.
24   Q. Yang, W. Xu, S. Gong, G. Zheng, Z. Tian, Y. Wen, L. Peng, L. Zhang, Z. Lu, L. Chen, *Nat. Commun.*, 2020, **11**, 5478.